Geochemistry Geophysics Geosystems G3
AN ELECTRONIC JOURNAL OF THE EARTH SCIENCES
Published by AGU and the Geochemical Society

Article
Volume 5, Number 8
5 August 2004
Q08H13, doi:10.1029/2003GC000661
ISSN: 1525-2027

Paleomagnetic results from the Snake River Plain: Contribution to the time-averaged field global database

Lisa Tauxe, Casey Luskin, and Peter Selkin
Scripps Institution of Oceanography, La Jolla, California 92093, USA (ltauxe@ucsd.edu; cluskin@ucsd.edu; pselkin@ucsd.edu)

Phillip Gans and Andy Calvert
Department of Geological Science, University of California Santa Barbara, Santa Barbara, California 93106-9630, USA (gans@magic.ucsb.edu; calvert@magic.ucsb.edu)

[1] This study presents paleomagnetic results from the Snake River Plain (SRP) in southern Idaho as a contribution to the time-averaged field global database. Paleomagnetic samples were measured from 26 sites, 23 of which (13 normal, 10 reverse) yielded site mean directions meeting our criteria for acceptable paleomagnetic data. Flow ages (on 21 sites) range from 5 ka to 5.6 Ma on the basis of $^{40}Ar/^{39}Ar$ dating methods. The age and polarity for the 21 dated sites are consistent with the Geomagnetic Reversal Time Scale except for a single reversely magnetized site dated at 0.39 Ma. This is apparently the first documented excursion associated with a period of low paleointensity detected in both sedimentary and igneous records. Combining the new data from the SRP with data published from the northwest United States between the latitudes of 40° and 50°N, there are 183 sites in all that meet minimum acceptability criteria for legacy and new data. The overall mean direction of 173 normally magnetized sites has a declination of 2.3°, inclination of 61.4°, a Fisher concentration parameter (κ) of 58, and a radius of 95% confidence (α_{95}) of 1.4°. Reverse sites have a mean direction of 182.4° declination, −58.6° inclination, κ of 50, and α_{95} of 6.9°. Normal and reversed mean directions are antipodal and indistinguishable from a geocentric axial dipole field at the 95% confidence level. Virtual geomagnetic pole dispersion was found to be circularly symmetric, while the directional data were elongate north-south. An updated and corrected database for the northwestern U.S. region has been contributed to the Magnetics Information Consortium (MagIC) database at http://earthref.org.

Components: 9257 words, 15 figures, 5 tables.

Keywords: gyromagnetic remanent magnetization; paleointensity; paleosecular variation; Snake River Plain; time-averaged geomagnetic field.

Index Terms: 1521 Geomagnetism and Paleomagnetism: Paleointensity; 1522 Geomagnetism and Paleomagnetism: Paleomagnetic secular variation; 1532 Geomagnetism and Paleomagnetism: Reference fields (regional, global).

Received 6 November 2003; **Revised** 13 April 2004; **Accepted** 16 June 2004; **Published** 5 August 2004.

Tauxe, L., C. Luskin, P. Selkin, P. Gans, and A. Calvert (2004), Paleomagnetic results from the Snake River Plain: Contribution to the time-averaged field global database, *Geochem. Geophys. Geosyst.*, *5*, Q08H13, doi:10.1029/2003GC000661.

Theme: Geomagnetic Field Behavior Over the Past 5 Myr

1. Introduction

[2] The fundamental assumption of many paleomagnetic studies is that the geomagnetic field, when averaged over sufficient time is well represented by a geocentric axial dipole (GAD). Yet recent compilations of paleomagnetic data suggest that there are long-lived nondipolar features of the field [*Schneider and Kent*, 1990; *Gubbins and Kelly*, 1993; *Quidelleur et al.*, 1994; *Johnson and Constable*, 1995]. Whether or not these nondipolar components are real or are artifacts of inadequate temporal sampling, imprecise paleomagnetic measurement techniques, or simple rock magnetic noise is a question which must be answered.

[3] The Time Averaged Field (TAF) initiative has begun to update the database of geomagnetic observations over the last five million years [see, e.g., *Mejia et al.*, 2002; *Tauxe et al.*, 2003] for 10 degree latitude bands up the Americas. The purpose of the present paper is to compile and augment the data from the northwestern sector of North America, between the latitude bands of 40 and 50°.

2. Previous Work in the Region

[4] Several paleomagnetic studies [*Brown and Mertzman*, 1979; *Mitchell et al.*, 1989; *Champion*, 1980] and a compilation by *Hagstrum and Champion* [2002] have been published from the northwestern United States between 40°N and 50°N (see Figure 1 for locations). For the purposes of this paper, we have submitted these data sets to the MagIC PMAG database on http://earthref.org.

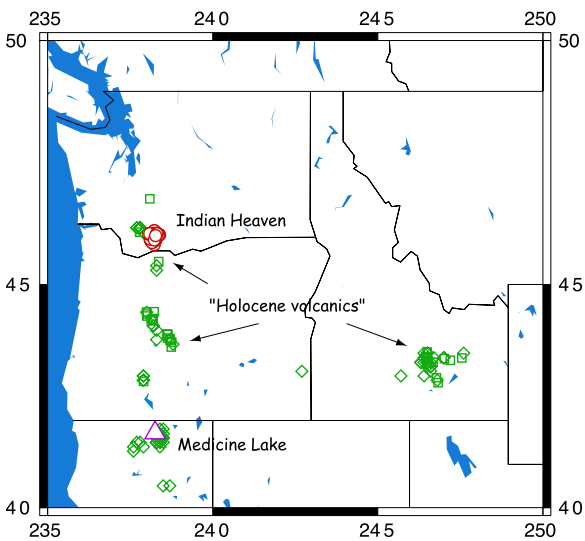

Figure 1. Map showing locations from published paleomagnetic studies in the NW United States (between 40° and 50°N latitude).

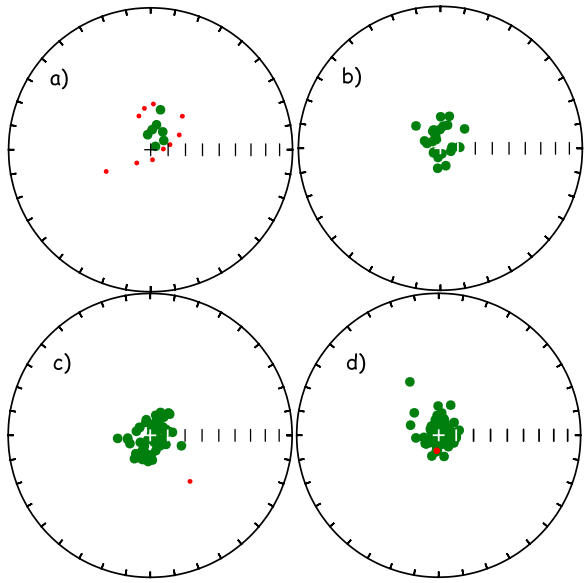

Figure 2. Equal area projections showing site mean paleomagnetic directions from all original published data from published paleomagnetic studies from the NW United States. The center of the diagram is the expected direction at each site. Smaller symbols are sites with $\kappa < 100$. (a) Results from Medicine Lake Lavas, N. California [*Brown and Mertzman*, 1979]. (b) Results from Indian Heaven Volcanic Field, Washington [*Mitchell et al.*, 1989]. (c) Results from western USA Holocene Volcanics [*Champion*, 1980]. (d) Results not included in Figure 2c reported by *Hagstrum and Champion* [2002].

[5] *Brown and Mertzman* [1979] studied the Medicine Lake Highland basaltic lavas of northern California (see Figures 1 and 2a). All 21 sites were normally magnetized and the oldest K-Ar date was 0.52 ± 0.21 Ma, consistent with a Brunhes age. The directional data are plotted in Figure 2a using the transformation of *Hoffman* [1984], which places the expected GAD direction ($\langle D \rangle = 0°$, $\langle I \rangle = 61°$) at the center of the diagram. For example, in this projection, data plotting in the upper half of the diagram are "too shallow" and in the right half are "right handed." The mean direction of the Medicine Lake lavas is $\bar{D} = 3.8°$ and $\bar{I} = 51.1°$ ($\alpha_{95} = 5.4°$ and $\kappa = 35$). This is far-sided and "right handed" with an inclination anomaly, ΔI, of $-11.5°$ from the expected inclination. The authors concluded that "the magnetic field is eccentric in the western United states to a degree not explained by current models" [*Brown and Mertzman*, 1979].

[6] *Tauxe et al.* [2003] examined the usefulness of various parameters as a means of selecting data in

their study of lava flows from the southwestern United States. They concluded that excluding sites with Fisher precision parameters of less than 100 and sites with fewer than 5 separately oriented samples eliminated the most deviant directions. The 14 sites in the *Brown and Mertzman* [1979] data set that fail these criteria are indicated by smaller symbols in Figure 2a. While it is true that the most deviant directions in the *Brown and Mertzman* [1979] data set have the lowest values of κ, the average direction of the seven remaining sites is still shallower than the GAD expectation ($\langle D \rangle = 5.7$, $\langle I \rangle = 49.9$, $\alpha_{95} = 5.6$).

[7] *Mitchell et al.* [1989] sampled the Plio-Pleistocene basalts of the Indian Heaven Volcanic field in the High Cascade region of southern Washington (see Figures 1 and 2b). All 57 sites from 23 units were normally magnetized, leading them to hypothesize that the K-Ar ages of the sites extending back to 3.75 Ma were questionable and that all of the data were actually of Brunhes age (0.78 Ma to present). The mean direction of the study was $\bar{D} = 3.6°$, $\bar{I} = 65.6°$ with an α_{95} of 2.6°. These directions are indistinguishable from a GAD field ($\langle I \rangle = 64°$). Only one site had $\kappa < 100$. Excluding this single site, the resulting mean direction is $\bar{D} = 2.6°$, $\bar{I} = 65.2°$ with an α_{95} of 2.5°.

[8] *Champion* [1980] conducted a paleomagnetic survey of Holocene lava flows in the western United States, including 29 within our study region (see Figures 1 and 2c). Rocks were dated using ^{14}C and indirect tree ring correlation. All sites are of Holocene age, and are normally magnetized. The mean direction is $\bar{D} = 359.4°$, $\bar{I} = 58.6°$ with an α_{95} of 3.0°, very close to the direction expected from a GAD field. All sites pass the *Tauxe et al.* [2003] criteria.

[9] *Hagstrum and Champion* [2002] compiled 94 estimates of the paleofield from 446 individual volcanic sites that had been dated by dendrochronology, ^{14}C or historical context (diamonds in Figure 1). We eliminated those sites duplicated by *Champion* [1980] and converted the remaining sites to directions. 72 of the remaining data points were taken from locations within the region considered here. 49 of these were averages of multiple sites as opposed to averages of multiple samples from a given site as in the other studies. The data were quoted as virtual geomagnetic pole (VGP) positions with most having an associated A_{95} and estimated κ. However, 24 VGPs were based on single sites and had no uncertainties quoted. All but one of the VGPs with κ estimates had κs well in excess of 100. We plot the transformed directions in Figure 2d). Removing the single demonstrably scattered site gives a mean direction of $\bar{D} = 1.8°$, $\bar{I} = 61.0°$ with an α_{95} of 1.9°, or indistinguishable from the expected direction.

[10] Despite the large data set available that meets minimum standards for acceptability, several aspects of the data suggest that more data are desirable. First, the age distribution of the data set is heavily skewed to the very recent past because of the preponderance of Holocene data in the large studies of *Champion* [1980] and *Hagstrum and Champion* [2002]. While a dominantly GAD field is not in question for the last 10,000 years or so, the character of the time-averaged field may be quite different. Secondly, there are no reversely magnetized sites and one persistent question is whether the normal and reverse fields are different [see, e.g., *Schneider and Kent*, 1990]. In this paper we present new data from 26 sites in the Snake River Plain volcanics, spanning the last five million years from both normal and reversely magnetized lava flows.

3. Geological Setting

[11] The Snake River Plain (SRP) is a 100 km wide crescent-shaped topographic depression that extends east-southeast from eastern Oregon to southern Idaho and then east-northeast from southern Idaho to the Idaho-Wyoming border near Yellowstone (see Figure 3). Its surface morphology is dominated by Pliocene to Recent basaltic lava flows, shield volcanoes, and rare rhyolitic domes. The basaltic lavas of the SRP are estimated to be >2 km thick in the central part of the plain [*Kuntz et al.*, 1992] and overlie rhyolitic ignimbrites and flows associated with the late Miocene to Pliocene transgressive sweep of the Yellowstone hotspot [*Hughes et al.*, 1999]. According to *Greeley and King* [1975], the SRP is divided into eastern and western structural sections which meet at 114° 30 W longitude near Twin Falls, Idaho. Early studies suggested that the eastern and western SRP shared a common history, though *Greeley and King* [1975] note that the western SRP is now thought to be a true graben-like structure, while the subsidence of the eastern SRP has a more complex history that is not well understood. The interior of the eastern SRP is a down-dropped aseismic zone, bounded by a highly faulted para-

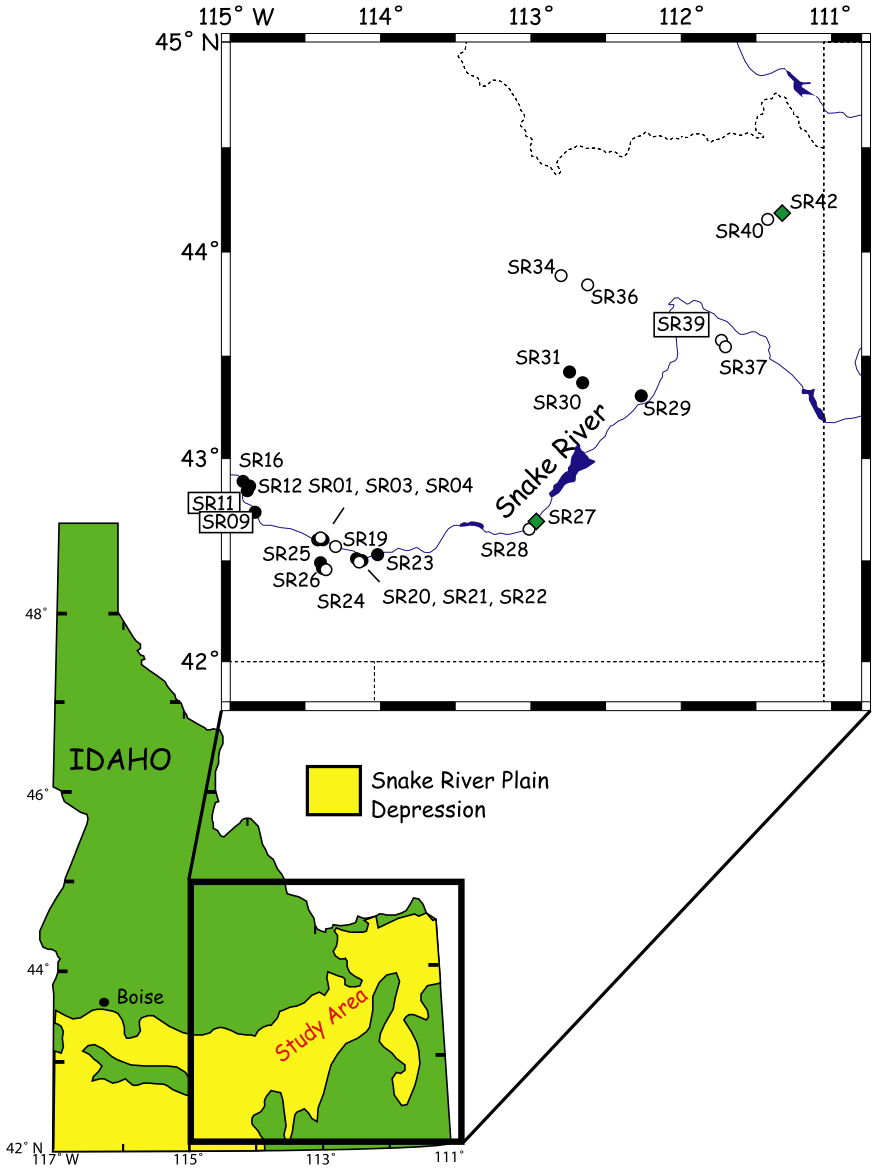

Figure 3. Locations of all sites sampled by this study in the Snake River Plain. Open (closed) symbols are reverse (normal). Diamonds are sites that fail to meet the minimum criteria.

bolically shaped zone [*Anders et al.*, 1989]. Some [*Scott et al.*, 1985a, 1985b; *Smith et al.*, 1985] have attributed the seismicity and tectonic forces which shaped the plain to crustal heating from the Yellowstone hotspot. Late Quaternary and Holocene basaltic centers and lava fields are widely scattered across the Snake River Plain and show no clear spatial trends [*Hughes and Thackray*, 1999]. Small, low-relief, monogenetic centers produce overlapping flows and, due to the subdued relief of the plain, typically only the youngest (<600 ka) flows are exposed at the surface. The older (early Quaternary and Pliocene) history of basaltic volcanism on the Snake River Plain is poorly known owing to this extensive cover. Samples from drill core, uplifted exposures along the margins of the plain, and within the deeply incised Snake River Gorge, suggest the overall character and spatial distribution of basaltic volcanism has resembled the Recent activity since perhaps the latest Miocene [*Hughes and Thackray*, 1999; *Calvert and Gans*, 2000]. New paleomagnetic samples were taken from 26 sites, mainly in the central part of the SRP in southern Idaho during September of 1999 (see Table 1 and Figure 3). These samples were collected from young flows exposed at the surface of the plain as well as from older lavas exposed on the southern boundary of the SRP and from the walls of the Snake River Gorge in the vicinity of Twin Falls, in order to get a representative sam-

Table 1. Site Locations and Summary Statistics for Paleomagnetic Sites Shown in Figure 3[a]

Site	Lat., N	Long., E	$\bar{D}$	$\bar{I}$	α_{95}	N_l	N_p	κ	Pol.	VGP. Lat.	VGP Long.
sr01	42.60264	245.60245	330.1	64.9	2.3	8	0	581.5	N	68.6	47.2
sr03	42.60352	245.5993	151.8	−57.5	3	7	0	405.3	R	−68.2	202.1
sr04	42.60104	245.59638	16.5	54.6	4.3	5	0	316.1	N	75.1	229.5
sr09	42.73656	245.16456	14.6	77.9	3	6	1	410.5	N	63.6	125.5
sr11	42.8418	245.11175	346.5	73.7	3	5	2	430.3	N	71.2	93.4
sr12	42.8657	245.12742	15.3	44.8	5.1	5	0	227.6	N	69.4	252.7
sr16	42.88822	244.92279	347.4	65.6	4	7	0	227.9	N	79.9	58.2
sr19	42.56857	245.70095	169.3	−63.5	2.7	4	0	1197.9	R	−81.9	226
sr20	42.49964	245.84815	334.3	51	8.6	8	0	42.2	X	68.9	9.4
sr21	42.49962	245.85094	172.4	−66.9	2.7	5	0	797.1	R	−81.2	259.9
sr22	42.50001	245.84971	6.3	29.7	3.3	6	1	335.5	N	62.9	280.7
sr23	42.52872	245.97898	14	46.6	2.9	5	1	565	N	71.5	251.8
sr24	42.45559	245.63636	163.3	−62.2	4.2	5	0	325.8	R	−77.8	214.8
sr25	42.48923	245.60009	2.9	61.9	2.6	5	0	871.8	N	87.8	186.9
sr26	42.46186	245.61471	358.6	62.4	5	6	1	153.1	N	88.6	47.1
sr27	42.69156	247.03567	230	70.6	4.7	2	3	350	X	16.9	85.4
sr28	42.65289	246.98823	195.8	−50.6	2.6	7	0	535.2	R	−72.7	60.1
sr29	43.30504	247.73219	9.4	62.7	1.6	8	0	1244.7	N	82.8	190.6
sr30	43.36817	247.3447	7.5	66.7	2.7	7	0	488.6	N	81.9	144.3
sr31	43.42133	247.25587	23.2	54	1.3	8	0	1836.2	N	69.7	221.1
sr34	43.8859	247.19945	205.4	−48.9	2.4	7	1	564.7	R	−65.9	49
sr36	43.84273	247.30639	197.1	−63.8	4.3	5	1	258.5	R	−77.8	9.1
sr37	43.53289	248.29368	175.6	−53.9	6.4	4	1	150.4	R	−80.3	130.1
sr39	43.57494	248.26583	187.3	−47.7	5.3	5	1	167.5	R	−74.1	87.5
sr40	44.15663	248.57442	192.9	−60.7	4.2	5	0	328.1	R	−80.3	31.5
sr42	44.18629	248.67201	21.6	52.7	36.4	5	0	5.4	X	70	226.9

[a] $\bar{D}$ ($\bar{I}$) is the mean declination (inclination). α_{95} is the circle of 95% confidence. N_l and N_p are the number of lines and planes, respectively. κ is the estimated precision parameter. Pol. is the polarity: N is normal, R is reverse, and X failed to meet the acceptance criteria discussed in the text. VGP Lat. and Long. are the latitude (°N) and longitude (°E) of the virtual geomagnetic pole positions.

pling for the last 5 Ma. Most of the flows sampled were basalts, although at least 3 were silicic tuffs. Samples from 21 of the 26 sites were also dated by the $^{40}Ar/^{39}Ar$ method. Preliminary geochronologic results for some of these sites were presented by *Calvert and Gans* [2000]. A detailed discussion of new $^{40}Ar/^{39}Ar$ geochronologic results for these and other samples and their implications for the history of basaltic volcanism of the central and eastern Snake River Plain will be presented elsewhere (P. B. Gans et al., manuscript in preparation, 2004). Here we briefly summarize the geochronologic results that bear directly on the paleomagnetic samples.

4. Methods

4.1. Sampling

[12] A total of 260 drill cores were taken from 26 sites in the SRP (Figure 3 and Table 1). All sites were individual lava flows chosen because of their accessibility and structural coherence. *Anders et al.* [1989] found that a parabolic ring of seismically distorted crust surrounds the eastern end of the SRP. The zone bounded by the parabola, where the SRP resides, is seismically undisturbed and suitable for paleomagnetic sampling without tectonic corrections. Care was taken during sampling to avoid areas possibly affected by some of the faults which extend from the parabolic zone into the SRP.

[13] Whenever possible, sites located at local lows in elevation were chosen because lightning would not tend to hit these areas and affect rock magnetization. Within each flow, samples were taken from blocks which appeared to be in situ.

[14] An average of 10 drill-core samples was taken per site using a water-cooled gas-powered portable rock drill. Samples were oriented using both magnetic and sun compass wherever possible. In most cases, the two agree within 5°. If sun compass measurements were not possible, magnetic directions were checked by "backsighting" using a Brunton compass. Backsiting is done by standing several meters away from the lava flow and aligning a second compass with the first to check for possible bias from the magnetization of the lava flow. The backsited directions are also typically within 5° of the original directions. Although this

method is cumbersome, it is sufficiently precise to correctly measure the azimuth of sample orientation to within 3°.

4.2. Paleomagnetic Methods

[15] Samples were usually between 8 and 12 cm in length and each sample was cut into approximately 3–4 individual specimens in the lab. Specimens were measured at the Scripps Institution for Oceanography Paleomagnetic Laboratory in a magnetically shielded room with an average field of approximately 200 nT. Specimens were measured on either a CTF or 2G cryogenic magnetometer.

[16] Demagnetizations were made using either thermal or alternating field (AF) demagnetization techniques. From each site, at least 5 specimens were chosen from different samples. Some underwent AF demagnetization while at least one per site underwent thermal demagnetization.

[17] AF demagnetization was carried out on a Sapphire Instruments SI-4 AF demagnetizer at 10 mT intervals to 40 mT, followed by 20 mT intervals to 180 mT or until the intensity dropped below 5% of the initial specimen intensity. After 40 mT, we employed a "double demagnetization" scheme whereby the specimens were demagnetized twice at a given field strength, once in the +x, +y, +z orientation, measured, and then demagnetized in the −x, −y, −z orientation and remeasured.

[18] Four specimens were treated to a triple demagnetization scheme (after completion of double demagnetization to 180 mT), whereby the specimens were demagnetized along +y, +z, +x, measured, then demagnetized along +*y*, measured and finally along +*z* and measured. This is the protocol of *Stephenson* [1993] to counteract the effect of gyroremanent magnetization (GRM) in anisotropic samples.

[19] The four "GRM" tested specimens were also subjected to an anisotropy of anhysteretic remanence (AARM) experiment [see *McCabe et al.*, 1985]. Specimens were first demagnetized in an AF field of 180 mT, then given an ARM in the first of the 15 positions described by *Jelinek* [1977]. Pairs of demagnetization and remagnetization measurements were then done in the other 14 positions.

[20] Thermal demagnetizations were conducted in a custom-built magnetically shielded oven capable of controlling temperatures to within 0.5°C. Specimens were demagnetized in 50° increments to 400°C after which we used 25° increments to 575°C. Specimens were evenly separated by approximately 1–2 cm inside the oven to ensure that the magnetization of stronger samples did not affect the magnetization of neighboring specimens during heating and cooling. Samples were initially heated rapidly to about 40°C below the set point, and held at that temperature for 10 minutes. The temperature was then slowly raised to the set point and held for approximately 20–30 minutes. This computer controlled "ramping method" avoids thermal overshoot and allows reproducibility of temperatures to within ~0.5°. After 20–30 minutes at the set point, the oven was turned off and specimens cooled by fan to room temperature at which point the specimens were measured.

[21] Fifty specimens from 12 sites were chosen for Thellier-Thellier analysis [*Thellier and Thellier*, 1959] to obtain absolute paleointensity data. In these experiments, specimens were heated to a given temperature step and allowed to cool in zero field. After measuring this "zero-field" step, the specimens were heated to the same temperature and allowed to cool in a 40 μT laboratory field applied along the specimen's "z" axis (in this case, along the length of the cylindrical specimens). At the 100, 200, 300, 400, 500, and 550° temperature steps, specimens were heated to a lower temperature and allowed to cool in the laboratory field. The difference between the first in-field step and the second (the so-called pTRM check step) is a measure of changes in the specimen's capacity to carry a TRM. Nine of the 50 Thellier experiments incorporated a so-called pTRM tail check [*Riisager and Riisager*, 2001] whereby a second "zero-field" step was performed after the in-field step. All heating steps were done in air.

4.3. $^{40}Ar/^{39}Ar$ Methods

[22] All of the samples were first carefully examined petrographically to determine which were sufficiently fresh and had the least amount of glass in the groundmass. Samples for dating were generally collected from the interior portions of individual lava flows, approximately one third of the distance above the base of the flow, as experience has shown that the best geochronologic data is obtained from the more slowly cooled, holocrystalline interiors, rather than the quenched (glassy) margins. Those deemed suitable for dating were crushed and sieved to varying size fractions (100–200 μm to 300–500 μm, depending on the sample) and ultrasonically cleaned in de-ionized water.

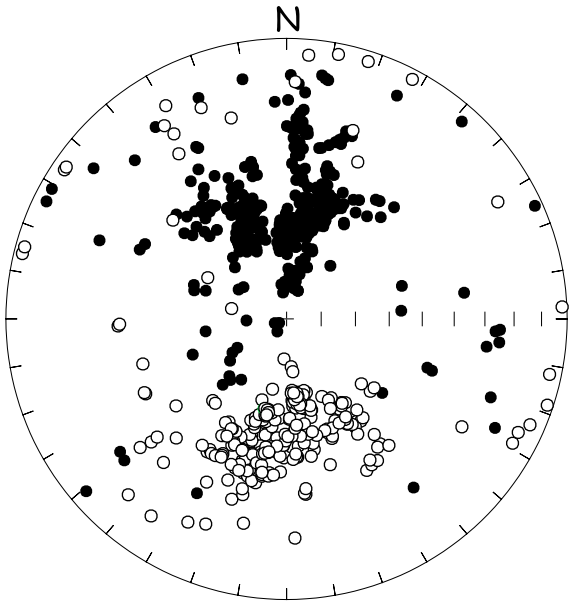

Figure 4. Equal area projection of all natural remanent magnetization (NRM) directions of all specimens. Open (closed) symbols are the upper (lower) hemisphere projections.

Standard magnetic separation techniques and hand picking were used to generate groundmass concentrates. Splits of each sample ranging from 50 to 200 mg were then encapsulated in copper packets and loaded into a sealed quartz vial interspersed with packaged flux monitors. Vials were irradiated in a cadmium-lined tube at the TRIGA reactor at Oregon State University in three separate irradiations for durations of 20 minutes to 1 hour depending on the estimated age of the sample. All samples were then analyzed by incremental heating in a Staudacher-type resistance furnace using the general procedures and system described by *Gans* [1997]. Analyses ranged from 8 to 15 step heating experiments for each sample. Our 22 new age determinations are summarized in Table 5. All errors given for our estimated (preferred) ages as reported throughout the text and in Table 5 are 2σ (95% confidence), and all older K-Ar ages have been recalculated for the new decay constants [*Steiger and Jager*, 1977]. A comprehensive discussion of this new geochronologic data, as well as for other samples from elsewhere on the Snake Rive Plain will be presented elsewhere (P. B. Gans et al., manuscript in preparation, 2004). The flux monitor used for all irradiations was Taylor Creek Rhyolite with an assigned age of 27.92 Ma [*Dalrymple and Duffield*, 1988]. For comparison, we obtain an age of 27.60 Ma on Fish Canyon Tuff Sanidine (another widely used standard) when we use Taylor Creek Rhyolite as our flux monitor.

5. Results

5.1. Directional Data

[23] NRM directions of all specimens are shown in Figure 4. Of the 26 sites 14 behaved as follows. Type I sites had NRMs that were initially well grouped (see Figure 5a) and remained well behaved through-out both thermal (Figure 5b) and AF (Figure 5c) demagnetization. Principal components [*Kirschvink*, 1980] could be fit to the characteristic directions with maximum angles of deviation (MADs) less than 5° resulting in a well defined site mean direction (Figure 5d). These sites are categorized as Type I. Ten sites fell into the category of Type II. These had NRMs that were initially quite scattered (Figure 6a), but achieved a well constrained site mean through progressive demagnetization. Type II specimens responded well to AF treatment, usually yielding a well-constrained characteristic direction by 10–20 mT (see Figure 6b) which was estimated with a best fit line. Thermal demagnetization was less effective, but revealed a great circle path (see Figure 6c). These data are fit with best fit planes [*Kirschvink*, 1980] which are acceptable if they have a MAD < 5°. Best fit directed lines and planes can be combined using the method of *McFadden and McElhinny* [1988] to establish a mean site direction, and associated Fisher parameters (see Figure 6d).

[24] The cause of the initial scatter in Type II sites could be lightning or some other form of overprinting. Given the relatively random directions of the scatter and the often high (>10 A/m) magnetization of samples from these sites, many of these are likely to be the result of lightning. Although other studies [e.g., *Tauxe et al.*, 2003] had difficulty removing the effects of lightning through thermal demagnetization, both thermal and AF demagnetization techniques were effective in this study in removing the overprints and isolating a component of the initial direction of magnetization. To qualify as Type II, we require a minimum of 4 directed lines (as opposed to planes) for acceptance of site mean and specimens from at least 5 separately oriented samples with MADs (for either lines or planes) of less than 5°.

[25] Four sites fail to qualify for either Type I or Type II designations. Two sites (sr20 and sr42) were similar to Type II sites in that the NRMs were scattered (Figure 7a), yet all demagnetization data

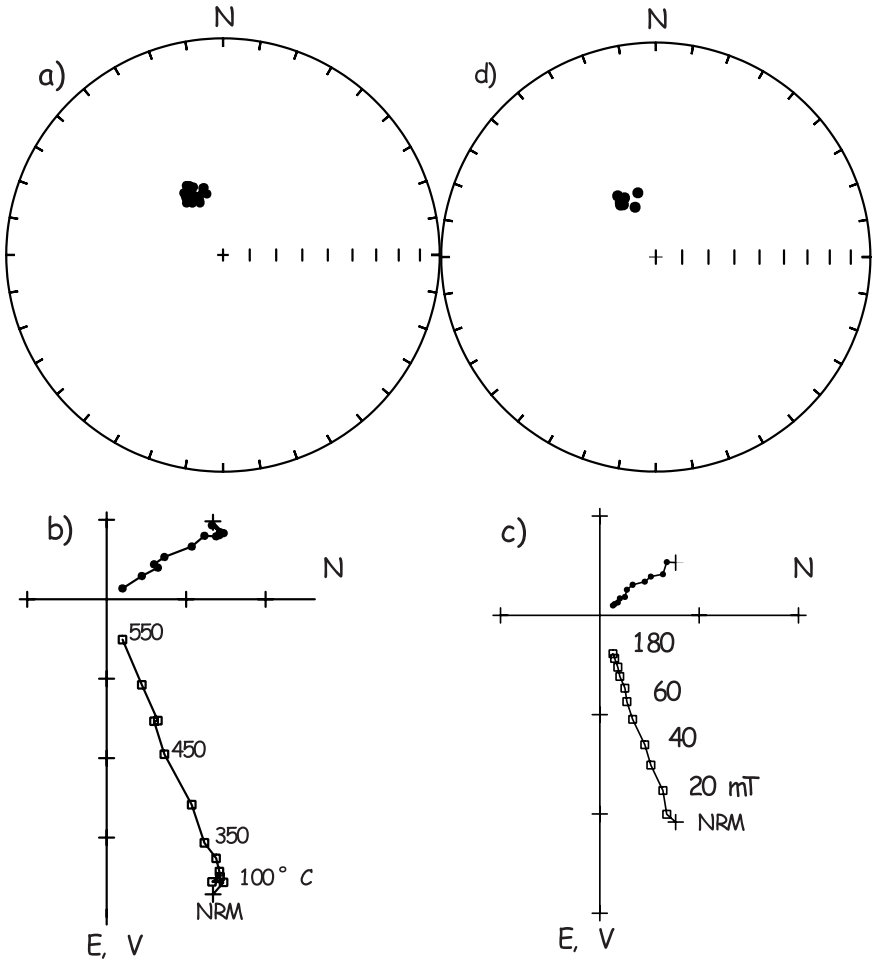

Figure 5. Representative Type I site (sr01). (a) Equal area projection of initial NRMs for all site specimens. NRMs are initially relatively closely grouped around a mean direction. (b) Vector endpoint diagram of progressive thermal demagnetization of specimen. Close (open) symbols are plotted on the horizontal (vertical) plane. (c) Same as Figure 5b for AF demagnetization. (d) Equal area projection of characteristic directions obtained for different specimens using principle component analysis.

yielded univectorial decay to the origin (see, e.g., Figure 7b), so no increase in concentration was observed. These we classify as Type III. The cause of this behavior could be error in orientation in the field of the outlying samples, rotation of the blocks from which the deviant samples were obtained, profound overprinting by lightning, or some other secondary magnetization. The median destructive fields for specimens from site sr42 ranged from ~10 mT to ~50 mT (see Figure 7c), much higher than frequently observed from lightning remanences. On the basis of field photos, neither block rotation nor incorrect orientation is a likely cause for the scatter. Thermal demagnetization behavior (see Figure 7d) indicates the presence of several magnetic phases, supporting the overprint hypothesis, however what sort of overprint in what sort of geomagnetic field remains unknown.

[26] Finally, two sites (sr27 and sr37) displayed strikingly different behavior and are classified Type IV. The NRM directions are well grouped (Figure 8a) and thermal demagnetization results in univectorial decay to the origin (Figure 8b). AF demagnetization using the double demagnetization technique, however, resulted in increasing divergence from the origin (Figure 8c).

[27] To investigate the cause of the Type IV behavior, we used the triple demagnetization using the protocol of *Stephenson* [1993]. In Figure 9 we show the three separate demagnetization steps (in specimen coordinates) for four specimens, two from Type I sites (sr01, sr03) and two from the two Type IV sites (sr27 and sr37). Type I sites show identical directions no matter how the specimen was demagnetized, while Type IV sites show

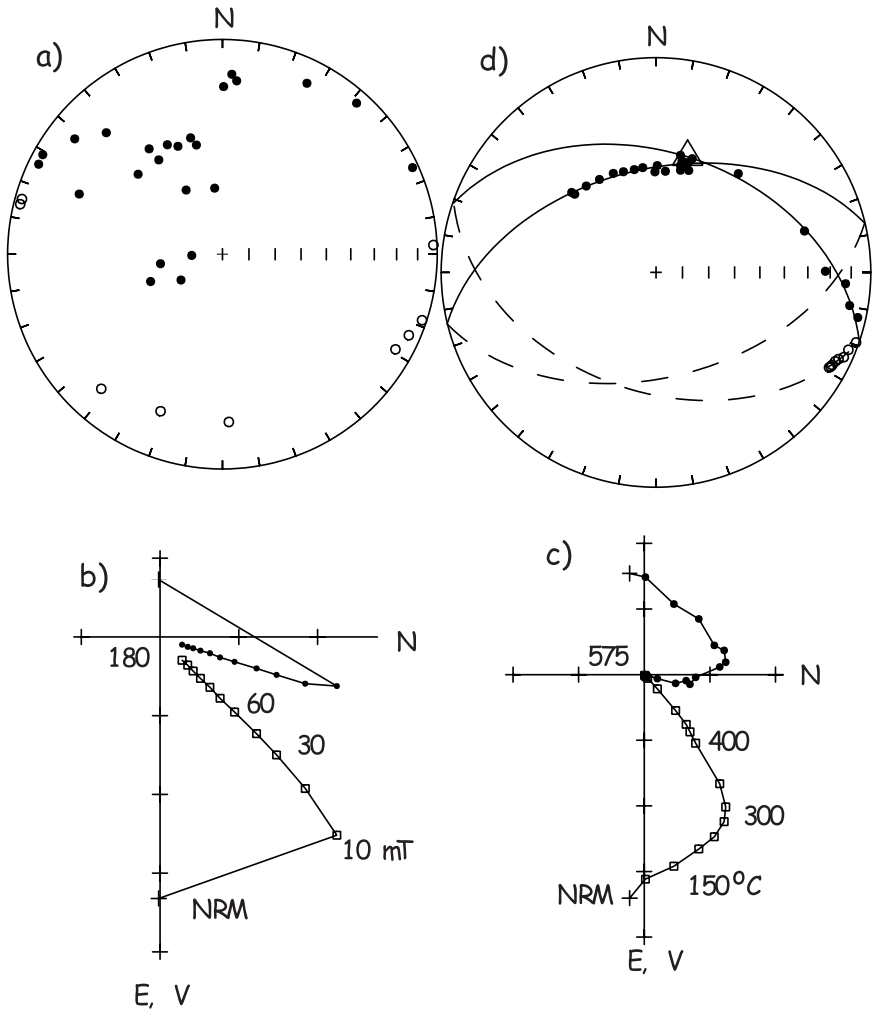

Figure 6. Representative Type II site (sr23). (a) Equal area projection of initial NRMs for all site specimens. NRMs are initially scattered. (b) Vector endpoint diagram of progressive AF demagnetization of specimen. (c) Vector endpoint diagram of progressive thermal demagnetization of specimen. (d) Equal area projections of demagnetization behavior of all specimens investigated from site. Some data are best interpreted as great circles and some are well fit by a line. These lines and planes can be combined using the technique of *McFadden and McElhinny* [1988] to estimate the mean direction (triangle) and associated *Fisher* [1953] parameters.

large deviations between the three different demagnetization procedures. *Stephenson* [1993] has ascribed this behavior to the acquisition of "gyroremanent magnetization" (GRM) in anisotropic samples.

[28] To explore the origin of Type IV behavior further, we subjected the same four specimens shown in Figure 9 to an AARM experiment as described in section 4. The 15 measurements were reduced to a best fit symmetric 3x3 tensor as described by *Tauxe* [1998] for anisotropy of magnetic susceptibility. The eigenparameters of the best fit tensors are listed in Table 2 whereby the eigenvalues are τ_i with τ_1 being the maximum and the associated eigenvectors are $\mathbf{V}_i$ using the terminology of *Tauxe* [1998]. The eigenvalues (τ) (scaled such that they sum to unity) of the best fit tensor can be plotted on a ternary diagram (see *Tauxe* [1998]) as shown in Figure 10. The use of the ternary diagram shows the degree of anisotropy (distance from the center of the diagram and labeled "sphere") and shape (oblate, prolate, etc.). The axes of the diagram shown to the right are elongation ($E' = \tau_1 + 0.5\ \tau_3$) and roundness ($R = \sin(60)\tau_3$). The two Type I sites are essentially isotropic with anisotropies ($100(\tau_1-\tau_3)$ of <2%, while the two Type IV sites are significantly oblate with anisotropies of ~9%.

[29] On the basis of the GRM and AARM results, the origin of the Type IV behavior is GRM

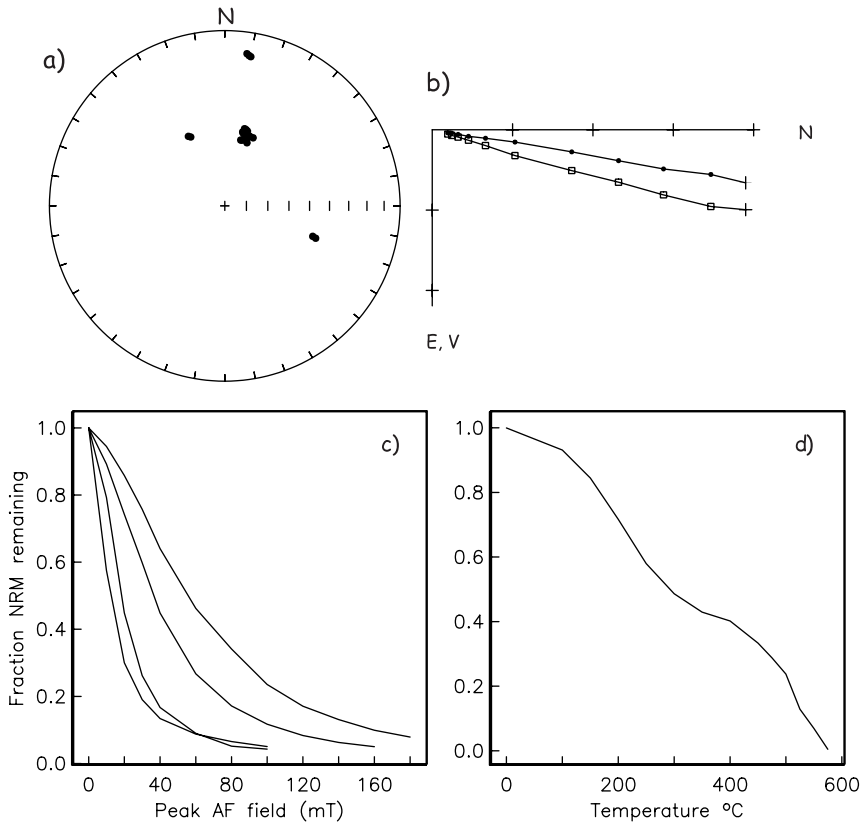

Figure 7. Site sr42 (Type III). (a) Equal area projection of initial NRMs for all site specimens from sr42. NRMs are scattered. (b) Vector endpoint diagram of progressive AF demagnetization of specimen. (c) Intensity decay of specimens during AF demagnetization. (d) Intensity decay of specimens during thermal demagnetization.

acquired during AF demagnetization in anisotropic specimens. One site (sr37) yielded sufficiently well behaved demagnetization data (best fit lines from at least four samples) to pass the acceptance criteria adopted here. The other (sr27) did not.

[30] All site mean directions are tabulated in Table 1 along with the number of best fit lines (N_l) and planes (N_p) used to calculate them. We include the *Fisher* [1953] parameters of the 95% circle of confidence (α_{95}) and the concentration parameter (κ). We also convert the directions to their virtual geomagnetic pole (VGP) positions.

5.2. Paleointensity

[31] We show representative examples of the results of our Thellier-Thellier experiments in Figure 11. The key assumptions in a Thellier-Thellier experiment are that the characteristic component of the remanence is thermally blocked. The magnitude of the remanence is assumed to be proportional to the ancient applied field. We further assume that the acquisition of laboratory pTRMs is analogous to the original thermal remanence. Alteration of the sample after initial cooling can violate the first and second assumptions respectively. Furthermore, if the magnetic grains are too large (either vortex state or multi-domain), the second assumption can be violated because blocking and unblocking may not be reciprocal processes.

[32] The Thellier-Thellier experiment allows the calculation of any number of "quality control" parameters and a variety have been defined. In this study, we find the following parameters to be useful:

[33] 1. The Deviation of the ANGle (DANG) that the NRM component used in the slope calculations makes with respect to the origin.

[34] 2. The Maximum Angle of Deviation (MAD) of *Kirschvink* [1980] of that component.

[35] 3. The "scatter" parameter (β) which is the standard error of the slope σ (assuming uncertainty in both the pTRM and NRM data) over the

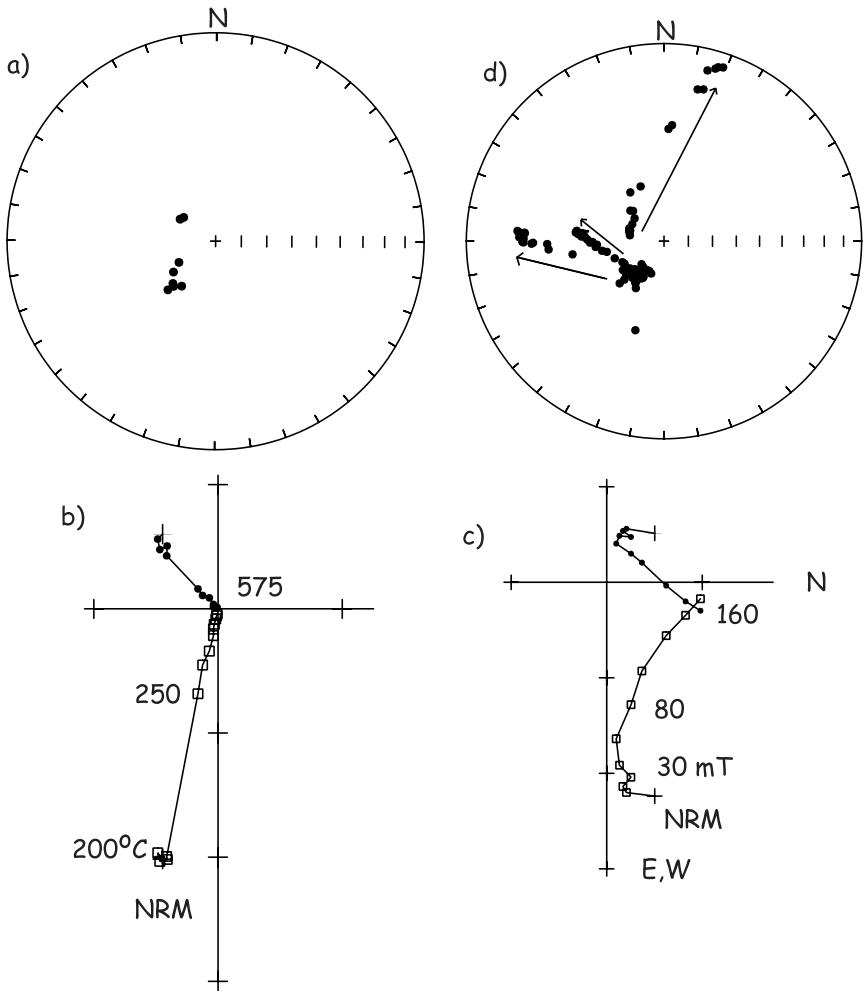

Figure 8. Example of Type IV site (sr27). (a) Equal area projection of initial NRMs for all site specimens. NRMs initially form a relatively well-constrained mean. (b) Vector endpoint diagram of progressive thermal demagnetization of specimen. (c) Vector endpoint diagram of progressive AF demagnetization. (d) Equal area projection of directions during demagnetization of specimens. Alternating field (AF) demagnetization tends to scatter the initially well-grouped directions, while thermal demagnetization leaves directions unchanged. Thus no reliable site mean can be established.

absolute value of the best fit slope $|b|$ [see *Coe et al.*, 1978].

[36] 4. *Coe et al.* [1978] advocated the use of the parameter f which is the fraction of the NRM component used in the slope estimation. We find that while f works well with single component magnetizations and reflects the fraction of the total NRM used in the slope calculation, it is misleading when there are multiple components. We use therefore a parameter f_{vds} which is the fraction of the total NRM, estimated by the vector difference sum (VDS) of the entire zero field demagnetization data. The VDS "straightens out" the various components of the NRM by summing up the vector differences at each demagnetization step.

[37] 5. The difference between the original pTRM at a given temperature step (horizontal component of the circles in Figure 11) and the pTRM check (horizontal component of the triangles in Figure 11), δ_i, can result from experimental noise or from alteration during the experiment. *Selkin and Tauxe* [2000] normalized the maximum δ_i value within the region of interest by the length of the hypotenuse of the NRM/pTRM data used in the slope calculation (the solid lines shown in Figure 11). DRAT is therefore the maximum difference ratio. In many cases, it is useful to consider the trend of the pTRM checks as well as their maximum deviations. We find therefore the sum of these differences $\Sigma\delta_i$ more useful than the maximum δ_i. Here, we normalize this difference sum by

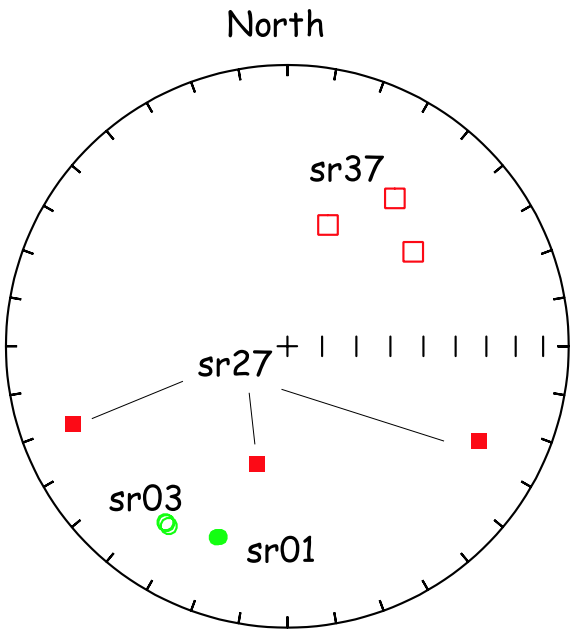

Figure 9. Equal area projections of the directions after the three AF demagnetization steps in the *Stephenson* [1993] GRM protocol. Circles are specimens from Type I sites, and squares are from Type IV sites (see text).

the pTRM acquired by cooling from the maximum temperature step used in the slope calculation to room temperature. This parameter is called the Difference RATion Sum or DRATS.

[38] The behavior of the Snake River Plain specimens, as characterized by the various quality parameters is illustrated in Figure 12. Most parameters show a clear inflection point separating "outlier" behavior from the rest. Inflections are marked for the βs at 0.15, the DANGs at 15°, the DRATSs at about 20%, the f_{vds}s at 0.4, and the MADs at 15°. Because there is no objective way of deciding the selection criteria for paleointensity data, we have chosen to use these inflection points as a guide for including data points at the site level. In addition, we have required there to be at least two pTRM checks prior to the maximum temperature step used and that the MD checks (where present) be less than 5%. We note that the complete data set has been archived in the MagIC repository at http://earthref.org so investigators can decide for themselves which criteria make the most sense in a different context. A total of 19 specimens from 6 sites meet these minimum criteria.

[39] Mean paleointensities were calculated for each site having specimens meeting the minimum criteria discussed above. Using a cutoff for the standard deviation of within site replicates of 15% yields four sites that meet this criterion. These are listed in Table 3.

[40] The average paleointensity from the four sites meeting minimum acceptance criteria is 53 μT with an equivalent axial dipole moment (ADM) of 88.6 ZAm^2 (see Table 4). This is significantly higher than the average of 55 $ZAm^2$for the last 5 million years of *Juarez and Tauxe* [2000]. However, two of the four sites are from the last 1 million years and one other (sr 39) is likely to be quite young given its easterly location. The single older site (sr01) has a paleointensity estimate (60 ZAm^2) that is closer to the long term average.

5.3. Ar/^{39}Ar Dating

[41] All sites meeting our minimal acceptance criteria were dated using $^{40}Ar/^{39}Ar$ techniques except for sites sr36, sr37, and sr38 (Table 5). Virtually all of the samples yielded reasonably well-behaved $^{40}Ar/^{39}Ar$ data with easily interpretable ages and uncertainties. Most of the samples yielded fairly flat age spectra having well defined plateaus or "pseudo plateaus" (Figure 13). Individual spectra range from "hump-shaped" to "U-shaped" to "L-shaped," a range of spectral types that is typical of fresh basalts and basaltic-andesites that have been dated from other localities [e.g., *Nauert and Gans*, 1994]. The shapes of these spectra and their deviation from an idealized flat plateau is readily explainable in terms of the combined effects but variable contributions of reactor-induced recoil, low temperature argon loss, and a nonatmospheric "trapped" component

Table 2. Results of the AARM Experiments[a]

Specimen	τ_3	D_{V_3}	I_{V_3}	τ_2	D_{V_2}	I_{V_2}	τ_1	D_{V_1}	I_{V_1}
sr01e2	0.3304	160.26	19.26	0.3332	297.28	64.47	0.3364	64.47	16.11
sr03d1	0.3242	28.04	83.50	0.3362	282.18	1.78	0.3397	191.98	6.25
sr27c1	0.2773	177.97	58.59	0.3595	74.66	8.00	0.3632	339.98	30.14
sr37j2	0.2832	157.82	39.53	0.3507	299.38	43.51	0.3661	50.00	20.35

[a] The τ_i are the eigenvalues, and the D_{V_i}, I_{V_i} are the eigenvector directions of the best fitting tensors in specimen coordinates.

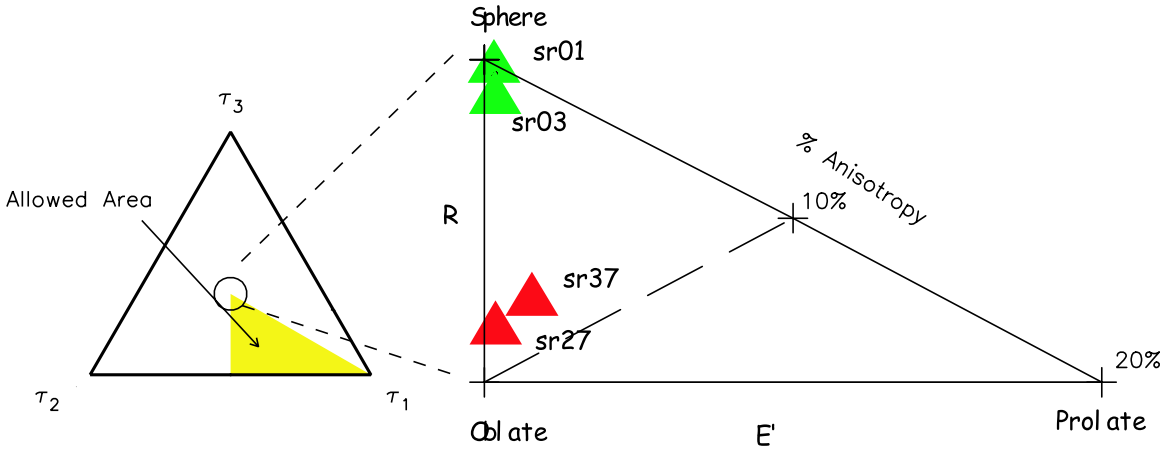

Figure 10. Projections of eigenvalues in a ternary diagram (see Table 2). Type I sites (sr01, sr03) are nearly isotropic, while the Type IV sites (sr27, sr37) are significantly oblate.

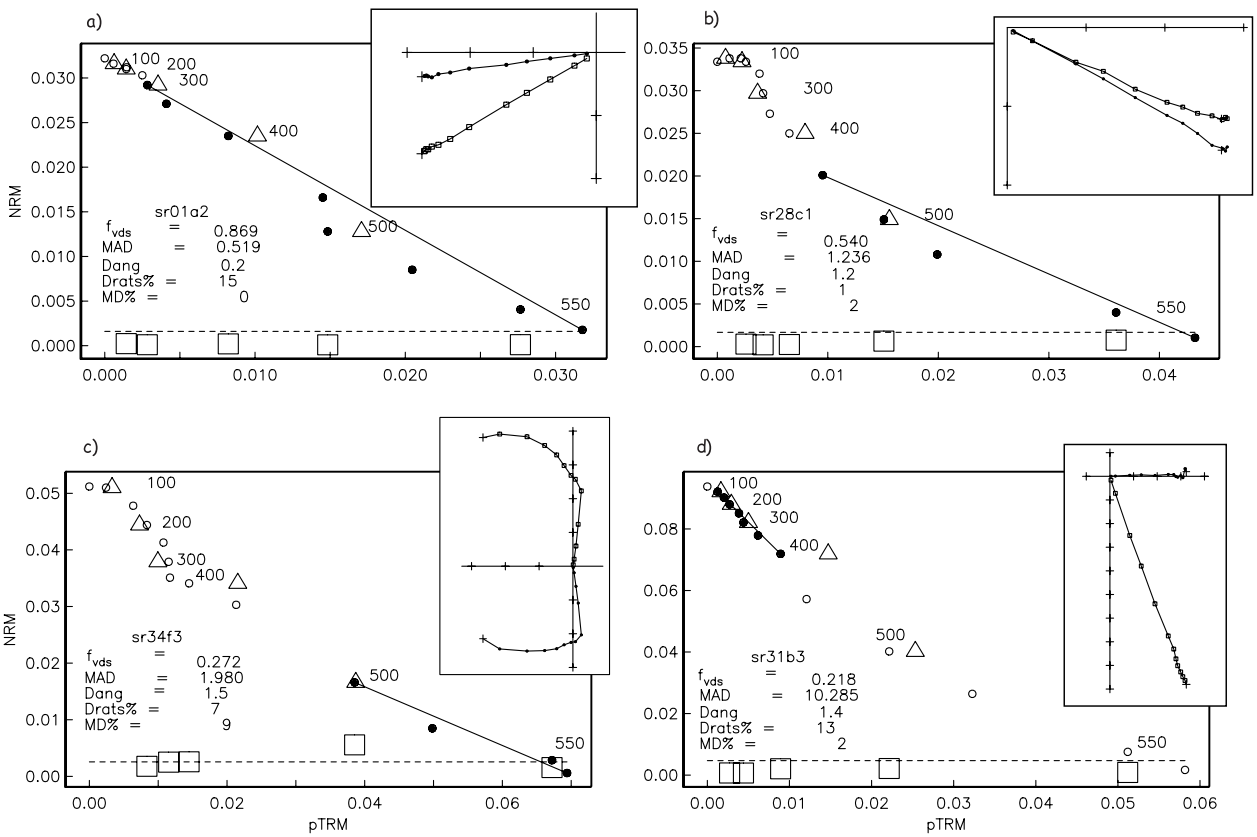

Figure 11. Representative Thellier-Thellier experiments. Solid symbols indicate data points used in calculation of slope. Triangles are pTRM checks. The difference δ between the pTRM component of the pTRM checks and the original measurement (circles), normalized by the length of the solid line, is the Difference RATio (DRAT). The sum of the δ_i prior to the maximum step used and normalized by the total pTRM acquired is DRATS. The squares are the differences in NRM between the first and second zero field measurements at a given step. The dashed line is 5% of the total NRM. The insets are the vector endpoint diagrams of the zero field steps. All data are in specimen coordinates. (a) Specimen sr01a2. Typical of the very best data. (b) Specimen sr28c1 has a somewhat lower value for f_{vds} than Figure 11a but still passes all selection criteria. (c) Specimen sr34f3. The f_{vds} is low owing to the multicomponent nature of the NRM. The maximum MD check exceeds the 5% line, suggesting that the specimen fails the reciprocity constraint for blocking and unblocking temperatures. (d) Specimen exhibits progressive alteration, and the usable portion of the data (<400C) is too short ($f_{vds} < 0.4$) for reliable paleointensity determination.

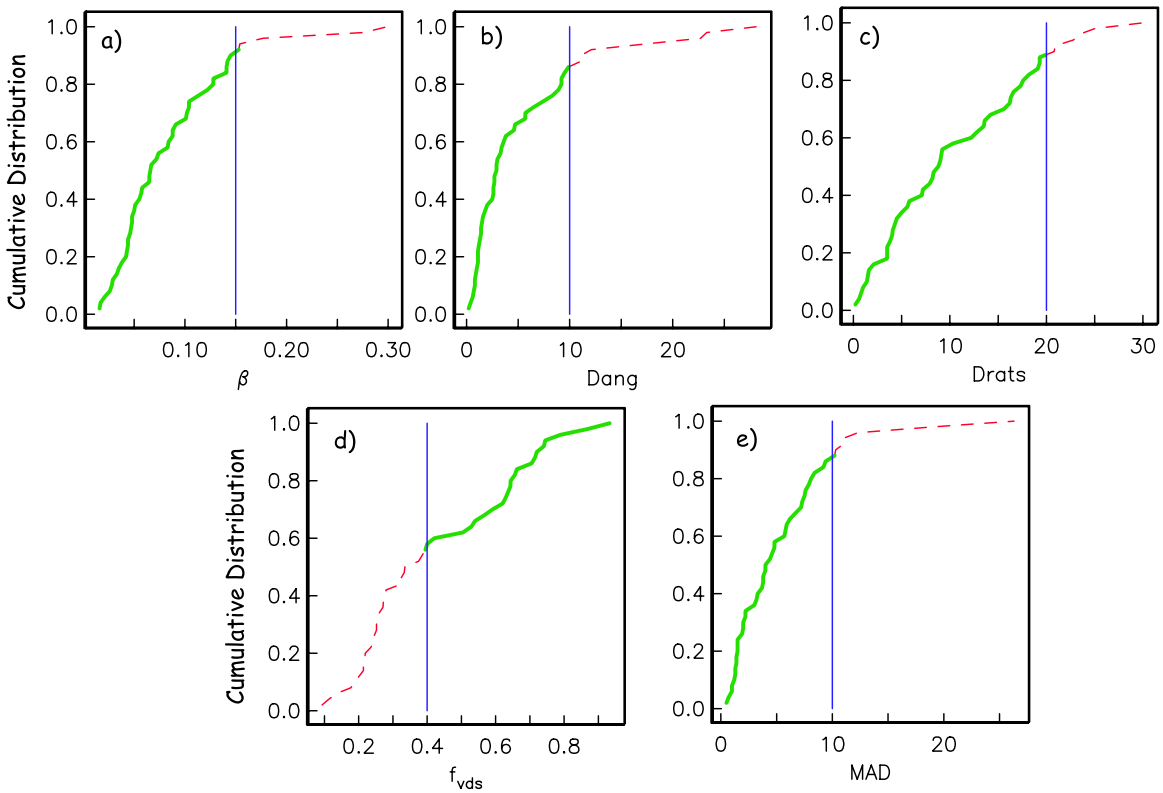

Figure 12. Cumulative distributions for various quality indices from the Thellier-Thellier experiments. The inflections are marked by solid lines and are used as cutoff values for the data presented here. The dashed portions of the data are excluded from the site averages (see text).

(i.e., excess argon). Reactor induced recoil [e.g., *Mankinen and Dalrymple*, 1972] tends to produce anomalously old apparent ages in the low temperature steps (e.g., Figure 13g) and may produce anomalously young ages in the high temperature steps. Argon loss due to hydration and clay alteration of groundmass glass tends to yield young apparent ages, especially in the low temperature steps (e.g., Figure 13a). Excess argon tends to be trapped in the early crystallized phenocryst phases (e.g., olivine, plagioclase) and is generally most evident in the highest temperature steps, associated with the lowest apparent K/Ca ratios (e.g., Figure 13c). All of these complications may be evident to varying degrees in a single sample (e.g., Figure 13g) but do not preclude a fairly precise assessment of the age. In particular, empirical studies by *Gans and Bohrson* [1998] on basalt samples whose ages are tightly bracketed by sanidine-bearing tuffs have shown that the age information from such spectra can be interpreted with a high degree of reliability. In particular, the reasonably flat central to high temperature part of the spectrum corresponding to the gas released from about 700°C to 950°C provides a fairly reliable estimate of the age, even if it does not constitute more than 50% of the gas released or strictly define a statistical plateau. In cases where the individual steps of this segment do not lie within two sigma analytical uncertainty of each other, we assign an uncertainty corresponding to one standard deviation of the selected ages a somewhat arbitrary assessment but one that has proven conservative in other studies [*Nauert and Gans*, 1994].

[42] Samples were collected from four groups of basalts (Banbury Basalt, Glenns Ferry Basalt, Idaho Group and Snake River Group) as mapped

Table 3. Summary of Paleointensity Results[a]

Site	N_B	$\bar{B}$ (μT)	$100 \times \sigma_B/\bar{B}$	VADM (ZAm^2)	σ_{VADM}
sr01	5	36.1	13.2	60.5	8.0
sr30	2	48.8	1.7	81.1	13.3
sr34	3	78.5	4.7	130	7.8
sr39	2	50.2	2.7	83.2	2.2

[a] N_B is the number of specimens used in the calculation of the average intensity $\bar{B}$ for each site. σ B is the standard deviation of the site average. VADM is the virtual axial dipole moment. Z is 10^{21}.

Table 4. Grand Means for the Northwestern U.S. Paleomagnetic Data[a]

Type of Average	$\bar{I}$	$\bar{D}$	α_{95}	N	κ	PP Lat.	PP Long.	A_{95}
Mean normal (SRP data)	59.7	6.0	7.6	13	30.6	86.2	340.3	9.0
Mean reverse (SRP data)	−58.6	182.4	6.9	10	50.1	−86.4	226.4	9.3
Grand mean (SRP data)	59.2	4.4	5	23	38.2	86.9	7.8	6.2
Mean normal (NWUS data)	61.5	2.3	1.4	173	58	88.5	353.6	1.
Grand mean (NWUS data)	61.35	2.3	1.4	183	58	88.6	1.0	1.8
Present direction	68.8	15.4						
GAD direction	−62	0						

		N	B (μT)	σ_B	ADM (ZAm^2)	σ_{ADM}
Grand mean intensity	dipole moment:	4	53.4	18.0	88.6	29.2

[a] 0–5 Ma.

by *Covington and Weaver* [1989, 1990, 1991] in the Snake River Canyon and several lavas from shields away from the canyon, including a few from the eastern Snake River Plain. For all samples, we analyzed groundmass concentrates of holocrystalline lavas. Typical confidence estimates range from 6–20 ka for <400 ka samples and 20–100 ka for 1–5 Ma samples. All samples with known stratigraphic context yielded ages in the correct order, thus strengthening our confidence in the reliability of these ages [*Calvert and Gans*, 2000]. Banbury Group basalts yielded ages of 5.1 ± 0.1 to 3.9 ± 0.1 Ma, substantially younger than previous K/Ar data of 8–14 Ma of *Armstrong et al.* [1975]. Glenns Ferry samples yielded ages of 3.83 ± 0.06 to 3.57 ± 0.02 Ma. Nine Idaho Group flows range in age from 3.4 ± 0.1 Ma to 291 ± 32 ka, each separated by 0.3 to 1.0 Ma. Basalts collected from shields on the surface of the plain in the vicinity of Twin Falls range in age from as old as 2.9 ± 0.1 Ma near the southern margin of the plain to 95 ± 10 ka. Thus Snake River Plain basalt flows exposed in and around the Snake River Canyon near Twin Falls record consistent, long-lived mafic volcanism from 5 Ma to the present, making it an ideal place to examine the time-averaged magnetic field over the past 5 Ma.

6. Discussion and Conclusions

[43] All sites except sr40 have ages and polarities that are consistent with the time scale of *Cande and*

Table 5. $^{40}Ar/^{39}Ar$ Dates

Site	Field Name	Age, Ma	2σ[a]	TFA	Isochron Age	Comment
sr01	Idaho Group-Qi10	3.40	0.06	3.47	3.41 ± 0.18 Ma	almost a plateau
sr03	Idaho Group-Qi7	2.0	0.10	2.14	2.07 ± 0.10 Ma	monotonically decreasing, but flat
sr04	Springs Basalt	0.095	0.010	0.087	89 ± 14 ka	nice plateau age
sr09	Springs Basalt	0.395	0.020	0.362	344 ± 124 ka	bouncy, but decent plateau
sr11	Malad Basalt	0.373	0.012	0.381	369 ± 16 ka	nice plateau age
sr12	Madson Basalt	0.404	0.014	0.402	0.408 ± 0.020	excellent plateau age
sr16	McKinney Basalt	0.052	0.024	0.138	96 ± 76 ka	loss profile, nice plateau
sr19	Idaho Group-Qi3	1.76	0.32	2.69	1.36 ± 0.28 Ma	extremely low radiogenic yields
sr20	Idaho Group-Qi12	2.26	0.10	2.13	1.84 ± 0.16 Ma	nice, minor plateau age
sr21	Idaho Group-Qi6	1.69	0.04	1.8	1.69 ± 0.12 Ma	nice plateau age
sr22	Idaho Group-Qi4	0.591	0.030	0.644	621 ± 158 ka	nice plateau age
sr23	Idaho Group-Qi1	0.291	0.032	0.295	304 ± 144 ka	nice plateau age, low radiogenic
sr24	Stricker Butte	1.73	0.02	1.87	1.74 ± 0.07 Ma	nice plateau age
sr25	Hubb Butte	2.89	0.04	3.08	2.94 ± 0.14 Ma	recoil pattern, but nice plateau
sr26	Hubb Butte (older)	2.94	0.05	3.09	2.98 ± 0.13 Ma	some recoil, near-plateau
sr28	Valley basalt	5.75	0.25	6.2	5.78 ± 0.28 Ma	monotonically decreasing
sr29	Hells Half Acre	0.184	0.028	0.101	204 ± 84 ka	hump shape with good flat
sr30	Taber Butte	0.191	0.016	0.227	71 ± 36 ka	Slight U shape, but fairly flat
sr31	Table Legs Basalt	0.124	0.078	0.271	302 ± 76 ka	low radiogenic, recoil
sr34	Circular Butte	0.945	0.06	1.115	930 ± 20 ka	massive recoil, small flat
sr40	Henry's Fork caldera	0.39	0.038	0.413	337 ± 90 ka	excellent plateau

[a] Uncertainties include the uncertainty in the flux parameter (J) but not in the absolute age of the flux monitor.

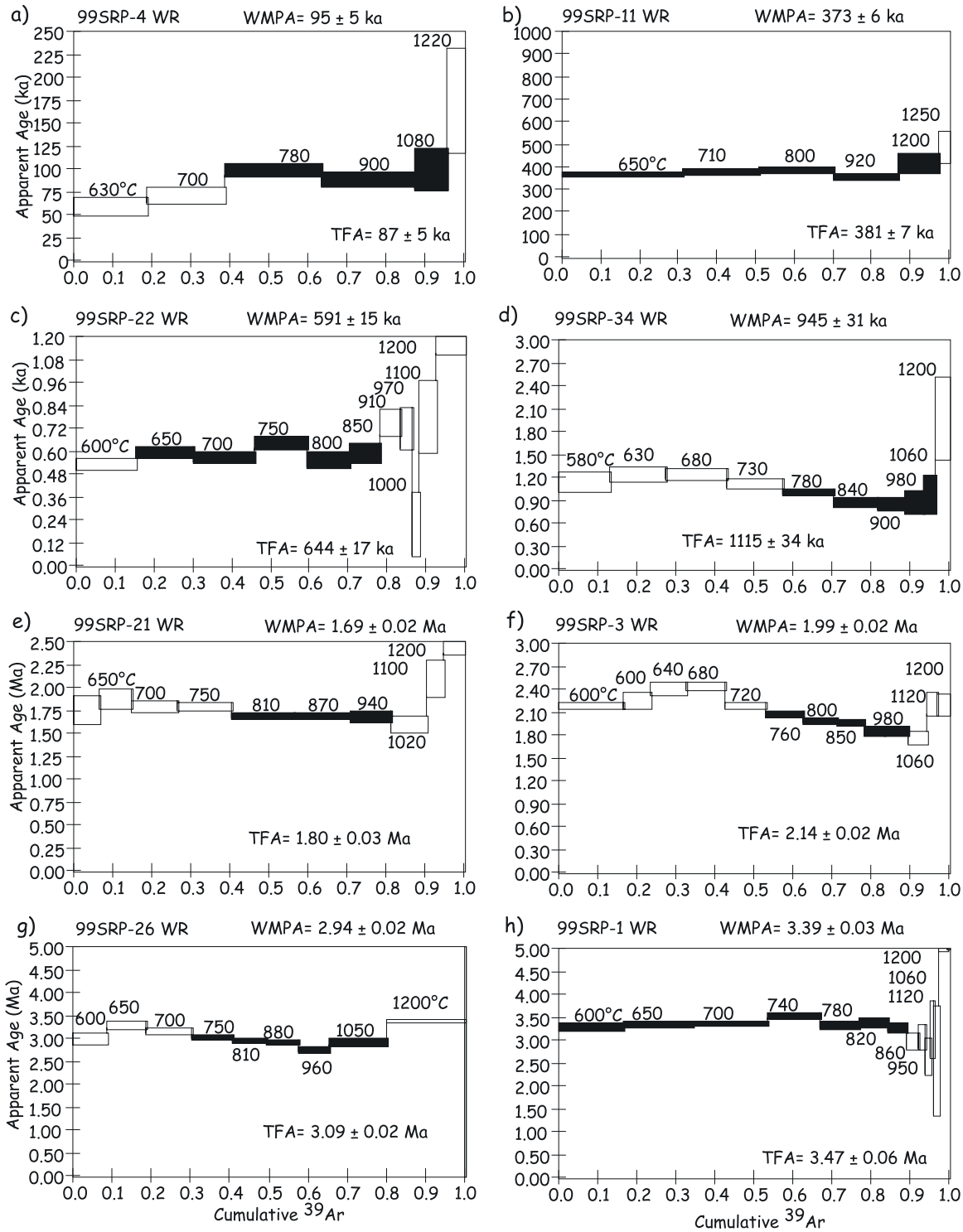

Figure 13. The $^{40}Ar/^{39}Ar$ age spectra for selected paleomagnetic samples from the Snake River Plain. All data from incremental heating experiments are plotted as apparent age of each temperature step versus the cumulative fraction of ^{39}Ar gas released. Steps used in the weighted mean plateau age calculation and are shaded black. Temperatures for each step are in °C. All errors (illustrated by each step thickness on the spectra and by the size of the boxes on the isochron plots) are estimated 1σ errors without the error in J (flux parameter).

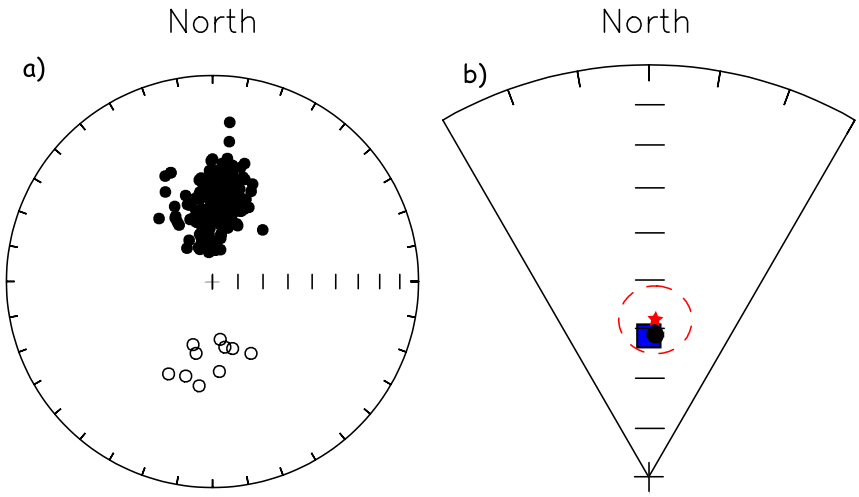

Figure 14. (a) Directions from site means passing minimum criteria from the northwestern U.S. sector. The normal data are not Fisherian but are somewhat elongate in the north-south direction. (b) Grand mean directions. Circle is the mean normal. The 95% confidence bound is smaller than the symbol. Star is the antipode of the mean reverse direction. The dashed line is its circle of 95% confidence. The square is the direction expected from a GAD field.

Kent [1995]. Site sr40 is reversely magnetized with an age of 0.39 ± 0.04 Ma. There are no commonly accepted "reversal excursions" in the Brunhes at this time. However, *Langereis et al.* [1997], *Guyodo and Valet* [1999], *Tauxe and Love* [2003], and *Channell and Raymo* [2003] all suggest low to very low paleofield intensities at this time. Perhaps site sr40 has recorded an elusive "Snake River Plain" excursion with fully reverse directions.

[44] *Tauxe et al.* [2003] evaluated acceptance criteria for a similar study from the southwestern United States for which there were approximately 700 sites. There are only 26 in the present study. This number is too few to use the approach taken in the *Tauxe et al.* [2003] study, so we have simply adopted their criteria ($N_{site} \geq 5$ and $\kappa \geq 100$) for the published data in the northwestern U.S. sector, except for the sites in the compilation of *Hagstrum and Champion* [2002] for which these data are uniformly not provided. For our new data, we have used the additional constraints that each site must have a minimum of four directed lines ($N_l \geq 4$ in Table 1). Using these criteria, we have a total of 183 sites of which 10 are reverse (see Figure 14a) and Table 1. We plot the means of the normal and antipodes of the reversely magnetized sites in Figure 14b as well as the direction expected from a GAD field. The three directions are indistinguishable. A Fisher distribution [*Fisher*, 1953] cannot be rejected for the few reversely magnetized sites (Figure 14a). The normal directions are not Fisher distributed, however as they are not circularly symmetric. The directional distribution is somewhat elongate north-south.

[45] The VGP positions from the data compiled in this paper are shown in Figure 15. The distribution of the VGPs is Fisherian and the

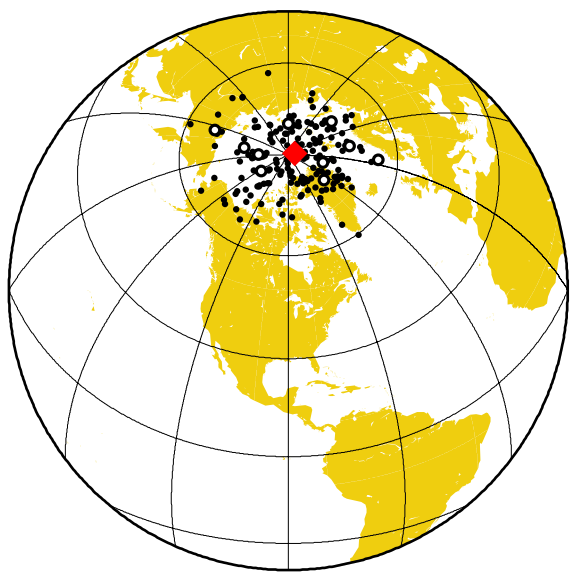

Figure 15. Virtual geomagnetic poles from the data shown in Figure 14a. The solid (open) symbols are the normal (antipodes of the reverse) VGPs. The diamond is the mean.

mean pole position is indistinguishable from the spin axis. This result is consistent with a field geometry with insignificant nonzero nonaxial dipole contributions.

Acknowledgments

[46] Andrew Newell, and Matt Cronin helped with sampling. Cathy Constable, Catherine Johnson and Jeff Gee provided useful discussions. Neil Opdyke, an anonymous reviewer and the Associate Editor, Dennis Kent, provided helpful reviews. We are grateful for funds provided to LT from grants NSF EAR9805164 and EAR 0003395.

References

Anders, M. H., J. W. Geissman, L. A. Piety, and J. T. Sullivan (1989), Parabolic distribution of circumeastern Snake River Plain seismicity and latest Quaternary faulting: Migratory pattern and association with the Yellowstone hotspot, *J. Geophys. Res.*, *94*, 1589–1621.

Armstrong, R., W. Leeman, and H. Malde (1975), K-Ar dating of Quaternary and Neogene volcanic rocks on the Snake River Plain, Idaho, *Am. J. Sci.*, *275*, 225–251.

Brown, L., and S. A. Mertzman (1979), Negative inclination anomalies from the Medicine Lake highland lavas, northern California, *Earth Planet. Sci. Lett.*, *42*, 121–126.

Calvert, A., and P. Gans (2000), $^{40}Ar/^{39}Ar$ chronology of 5 to 0 Ma central Snake River Plain basalts, *Eos Trans. AGU*, *81*(48), Fall Meet. Suppl., Abstract V21D-28.

Cande, S. C., and D. V. Kent (1995), Revised calibration of the geomagnetic polarity timescale for the late Cretaceous and Cenozoic, *J. Geophys. Res.*, *100*, 6093–6095.

Champion, D. E. (1980), Holocene geomagnetic secular variation in the western United States: Implications for the global geomagnetic field, *U.S. Geol. Surv. Open File Rep.*, *80–824*, 314–354.

Channell, J. E. T., and M. E. Raymo (2003), Paleomagnetic record at ODP Site 980 (Feni Drift, Rockall) for the past 1.2 Myrs, *Geochem. Geophys. Geosyst.*, *4*(4), 1033, doi:10.1029/2002GC000440.

Coe, R. S., S. Grommé, and E. A. Mankinen (1978), Geomagnetic paleointensities from radiocarbon-dated lava flows on Hawaii and the question of the Pacific nondipole low, *J. Geophys. Res.*, *83*, 1740–1756.

Covington, H., and J. Weaver (1989), Geologic map and profiles of the north wall of the Snake River canyon, Bliss, Hagerman, and Tuttle quadrangles, Idaho, *U.S. Geol. Surv. Misc. Invest. Ser.*, *Map I-1947-A*, scale 1:24,000.

Covington, H., and J. Weaver (1990), Geologic map and profiles of the north wall of the Snake River canyon, Pasadena Valley and Ticeska quadrangles, Idaho, *U. S. Geol. Surv. Misc. Invest. Ser.*, *Map I-1947-B*, scale 1:24,000.

Covington, H., and J. Weaver (1991), Geologic map and profiles of the north wall of the Snake River canyon, Thousand Springs and Niagara Springs quadrangles, Idaho, *U. S. Geol. Surv. Misc. Invest. Ser.*, *Map I-1947-C*, scale 1:24,000.

Dalrymple, G., and W. Duffield (1988), High-precision $^{40}Ar/^{39}Ar$ dating of Oligocene rhyolites from the Mogollon-Datil volcanic field using a continuous laser system, *Geophys. Res. Lett.*, *15*, 463–466.

Fisher, R. A. (1953), Dispersion on a sphere, *Proc. R. Soc. London, Ser. A*, *217*, 295–305.

Gans, P. (1997), Large-magnitude Oligo-Miocene extension in southern sonora— Implications for the tectonic evolution of northwest Mexico, *Tectonics*, *16*, 388–408.

Gans, P. B., and W. A. Bohrson (1998), Suppression of volcanism during rapid extension in the Basin and Range Province, United States, *Science*, *279*, 66–68.

Greeley, R., and J. S. King (1975), Geologic field guide to the Quaternary volcanics of the south-central Snake River Plain, Idaho, *Pamphlet 176*, Idaho Bur. of Mines and Geol., Moscow, Idaho.

Gubbins, D., and P. Kelly (1993), Persistent patterns in the geomagnetic field over the past 2.5 myr, *Nature*, *365*, 829–832.

Guyodo, Y., and J. P. Valet (1999), Global changes in intensity of the Earth's magnetic field during the past 800 kyr, *Nature*, *399*, 249–252.

Hagstrum, J. T., and D. E. Champion (2002), A Holocene paleosecular variation record from ^{14}C-dated volcanic rocks in western North America, *J. Geophys. Res.*, *107*(B1), 2025, doi:10.1029/2001JB000524.

Hoffman, K. (1984), A method for the display and analysis of transitional paleomagnetic data, *J. Geophys. Res.*, *89*, 6285–6292.

Hughes, S. S., and G. D. Thackray (Eds.) (1999), *Guidebook to the Geology of Eastern Idaho*, Idaho Mus. of Nat. Hist., Pocatello.

Hughes, S. S., R. P. Smith, W. R. Hackett, and S. R. Anderson (1999), Mafic volcanism and environmental geology of the eastern Snake River Plain, Idaho, in *Guidebook to the Geology of Eastern Idaho*, edited by S. S. Hughes and G. D. Thackray, pp. 143–168, Idaho Mus. of Nat. Hist., Pocatello.

Jelinek, V. (1977), Statistical processing of anisotropy of magnetic susceptibility measured on groups of specimens, *Stud. Geophys. Geod.*, *22*, 50–62.

Johnson, C. L., and C. G. Constable (1995), The time-averaged geomagnetic field as recorded by lava flows over the past 5 myr, *Geophys. J. Int.*, *122*, 498–519.

Juarez, M., and L. Tauxe (2000), The intensity of the time averaged geomagnetic field: The last 5 m. y., *Earth Planet. Sci. Lett.*, *175*, 169–180.

Kirschvink, J. L. (1980), The least-squares line and plane and the analysis of paleomagnetic data, *Geophys. J. R. Astron. Soc.*, *62*, 699–718.

Kuntz, M., H. Covington, and L. Schorr (1992), An overview of basaltic volcanism of the eastern Snake River Plain, Idaho, *Mem. Geol. Soc. Am.*, *179*, 289–304.

Langereis, C., M. Dekkers, G. de Lange, M. Paterne, and P. van Santvoort (1997), Magnetostratigraphy and astronomical calibration of the last 1.1 myr from an eastern Mediterranean piston core and dating of short events in the Brunhes, *Geophys. J. Int.*, *129*, 75–94.

Mankinen, E., and G. Dalrymple (1972), Electron microprobe evaluation of terrestrial basalts for whole-rock K-Ar dating, *Earth Planet. Sci. Lett.*, *17*, 89–94.

McCabe, C., M. Jackson, and B. B. Ellwood (1985), Magnetic anisotropy in the Trenton limestone: Results of a new technique anisotropy of anhysteretic susceptibility, *Geophys. Res. Lett.*, *12*, 333–336.

McFadden, P. L., and M. W. McElhinny (1988), The combined analysis of remagnetization circles and direct observations in paleomagnetism, *Earth Planet. Sci. Lett.*, *87*, 161–172.

Mejia, V., R. W. Barendregt, and N. D. Opdyke (2002), Paleosecular variation of Brunhes age lava flows from British Columbia, Canada, *Geochem. Geophys. Geosyst.*, *3*(12), 8801, doi:10.1029/2002GC000353.

Mitchell, R. J., D. J. Jaeger, J. F. Diehl, and P. E. Hammond (1989), Paleomagnetic results from the Indian Heaven volcanic field, south-central Washington, *Geophys. J.*, *97*, 381–390.

Nauert, J., and P. B. Gans (1994), $^{40}Ar/^{39}Ar$ geochronology of whole rock basalts, *Geol. Soc. Am. Bull. Abstr. Programs*, *26*, 76.

Quidelleur, X., J. P. Valet, V. Courtillot, and G. Hulot (1994), Long-term geometry of the geomagnetic field for the last five million years: An updated secular variation database, *Geophys. Res. Lett.*, *21*, 1639–1642.

Riisager, P., and J. Riisager (2001), Detecting multidomain magnetic grains in Thellier palaeointensity experiments, *Phys. Earth Planet. Inter.*, *125*, 111–117.

Schneider, D. A., and D. V. Kent (1990), The time-averaged paleomagnetic field, *Rev. Geophys.*, *28*, 71–96.

Scott, W. E., K. L. Pierce, and J. M. H. Hait (1985a), Quaternary tectonic setting of the 1983 Borah Peak earthquake, central Idaho, *Bull Seismol. Soc. Am.*, *75*, 1053–1066.

Scott, W. E., K. L. Pierce, and J. M. H. Hait (1985b), Quaternary tectonic setting of the 1983 Borah Peak earthquake, central Idaho, *U.S. Geol Surv. Open File Rep.*, *85*, 1–16.

Selkin, P., and L. Tauxe (2000), Long-term variations in paleointensity, *Philos. Trans. R. Astron. Soc.*, *358*, 1065–1088.

Smith, R. B., W. D. Richins, and D. I. Doser (1985), The 1983 Borah Peak, Idaho earthquake: Regional seismicity, kinematics of faulting, and tectonic mechanism, *U.S. Geol. Surv. Open File Rep.*, *85*, 236–263.

Steiger, R. H., and E. Jager (1977), Subcommission on geochronology: Conventions on the use of decay constants in geo- and cosmochronology, *Earth Planet. Sci. Lett.*, *36*, 359–362.

Stephenson, A. (1993), Three–axis static alternating field demagnetization of rocks and the identification of NRM, gyroremanent magnetization, and anisotropy, *J. Geophys. Res.*, *98*, 373–381.

Tauxe, L. (1998), *Modern Approaches in Geophysics*, vol. 17, *Paleomagnetic Principles and Practice*, Kluwer Acad., Norwell, Mass.

Tauxe, L., and J. J. Love (2003), Paleointensity in Hawaiian Scientific Drilling Project Hole (HSDP2): Results from submarine basaltic glass, *Geochem. Geophys. Geosyst.*, *4*(2), 8702, doi:10.1029/2001GC000276.

Tauxe, L., C. Constable, C. L. Johnson, A. A. P. Koppers, W. R. Miller, and H. Staudigel (2003), Paleomagnetism of the southwestern U. S. A. recorded by 0–5 Ma igneous rocks, *Geochem. Geophys. Geosyst.*, *4*(4), 8802, doi:10.1029/2002GC000343.

Thellier, E., and O. Thellier (1959), Sur l'intensité du champ magnétique terrestre dans le passé historique et géologique, *Ann. Geophys.*, *15*, 285–378.